Supporting information

Native Mass Spectrometry Dissects the Structural Dynamics of an Allosteric Heterodimer of SARS-CoV-2 Nonstructural Proteins

Stephanie M. Thibert[1,†], Deseree J. Reid[2,†], Jesse W. Wilson[1,†], Rohith Varikoti[3], Natalia Maltseva[4,5], Katherine J. Schultz[3], Agustin Kruel[3], Gyorgy Babnigg[4,6], Andrzej Joachimiak,[4,5], Neeraj Kumar[3], Mowei Zhou[1,⊥,*]

1. Environmental Molecular Sciences Laboratory, Pacific Northwest National Laboratory, Richland, WA 99354, United States
2. Chemical and Biological Signature Sciences, Pacific Northwest National Laboratory, Richland, WA 99354, United States
3. Biological Sciences Division, Pacific Northwest National Laboratory, Richland, WA 99354, United States
4. Center for Structural Biology of Infectious Diseases, Consortium for Advanced Science and Engineering, University of Chicago, Chicago, IL 60637, United States
5. Structural Biology Center, X-ray Science Division, Argonne National Laboratory, Argonne, IL 60439, United States
6. Biosciences Division, Argonne National Laboratory, Argonne, IL 60439, United States

† These authors contributed equally.
⊥ Present address: Department of Chemistry, Zhejiang University, Hangzhou, Zhejiang, 310058, China
Correspondence: moweizhou@zju.edu.cn

Table of Content

Supporting Table

Nsp10
SNMAGNATEVPANSTVLSFCAFAVDAAKAYKDYLASGGQPITNCVKMLCTHTGTGQAITVTPEANMDQESFGGAS CCLYCRCHIDHPNPKGFCDLKGKYVQIPTTCANDPVGFTLKNTVCTVCGMWKGYGCSCDQLREPMLQ
Nsp16
SNMSSQAWQPGVAMPNLYKMQRMLLEKCDLQNYGDSATLPKGIMMNVAKYTQLCQYLNTLTLAVPYNMRVIHF GAGSDKGVAPGTAVLRQWLPTGTLLVDSDLNDFVSDADSTLIGDCATVHTANKWDLIISDMYDPKTKNVTKENDSK EGFFTYICGFIQQKLALGGSVAIKITEHSWNADLYKLMGHFAWWTAFVTNVNASSSEAFLIGCNYLGKPREQIDGYV MHANYIFWRNTNPIQLSSYSLFDMSKFPLKLRGTAVMSLKEGQINDMILSLLSKGRLIIRENNRVVISSDVLVNN
Nsp10’
GHMAGNATEVPANSTVLSFCAFAVDAAKAYKDYLASGGQPITNCVKMLCTHTGTGQAITVTPEANMDQESFGGA SCCLYCRCHIDHPNPKGFCDLKGKYVQIPTTCANDPVGFTLKNTVCT VCGMWKGYGC SCDQLREPMLQ

Table S1. Sequences of nsp10, nsp16, and nsp10’.

Supporting Figures

(A) Deconvolved mass of the nsp10 and nsp16 monomers in the denatured sample

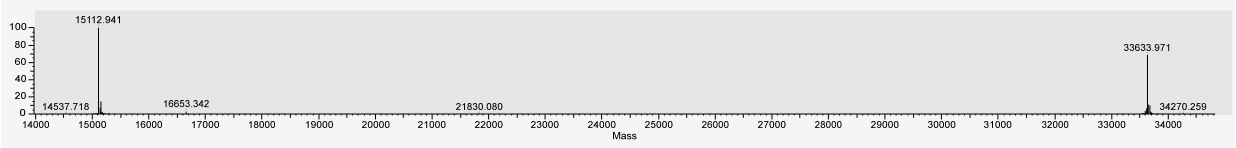

(B) Deconvolved mass of the nsp10 and nsp16 monomers in the nondenatured sample

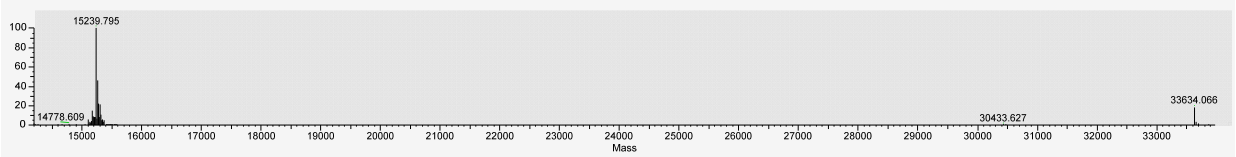

Figure S1. Monoisotopic masses of the nsp10 and nsp16 monomers under (A) denatured condition of 50:50 water: acetonitrile, and (B) nondenatured condition of 100 mM ammonium acetate. Protein concentration was 0.25 mg/mL. The spectra were collected with static nano electrospray on a Thermo Orbitrap Exploris 480 and UHMR, respectively, with resolution set to 240k (at *m/z* 200). Mass deconvolution was performed with Xtract in FreeStyle v1.5. Theoretical sequence masses of nsp10 and nsp16 are 15111.915 Da and 33633.866 Da, which are within 10 ppm (considering deisotoping error). The nsp10 mass in nondenaturing mode shifted by addition of two Zn ions.

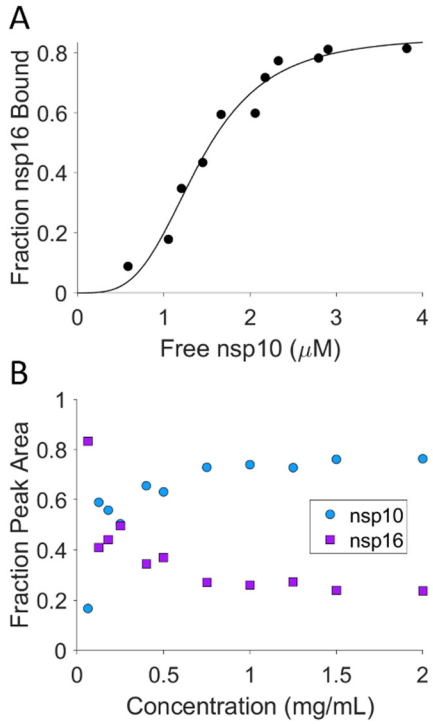

Figure S2. (A) Single-site binding followed a sigmoidal curve and was likely a reflection of the changes in ionization efficiency between nsp10 and nsp16 monomers and nsp10/16 dimer with changes in total protein concentration. Due to this limitation, our K_d calculation is an estimate rather than a precise quantification of nsp10/16 dimerization. (B) Ionization efficiency of nsp10 and nsp16 monomers at increased total protein concentrations.

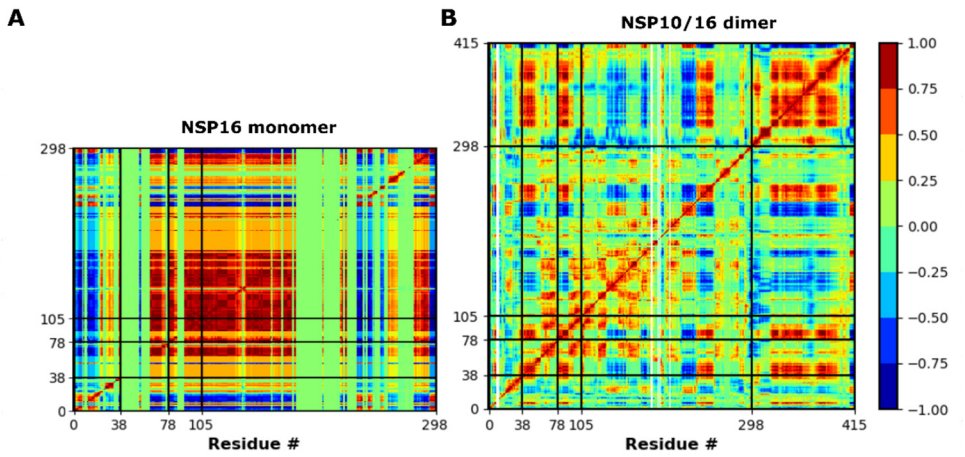

Figure S3. Dynamic cross-correlation matrix (DCCM) plot representing the residue-residue cross correlations (A) nsp16 monomer (residues: 0 – 298) and (B) nsp10/16 dimer (nsp16 residues: 0 – 298, (nsp10 residues: 299-415). The correlated (motions in same direction) and anti-correlated (motions in opposite direction) motions are color-coded, from dark red to green to blue. DCCM plot shows that several correlated motions which are available in the nsp16 monomer disappear upon dimerization with nsp10.

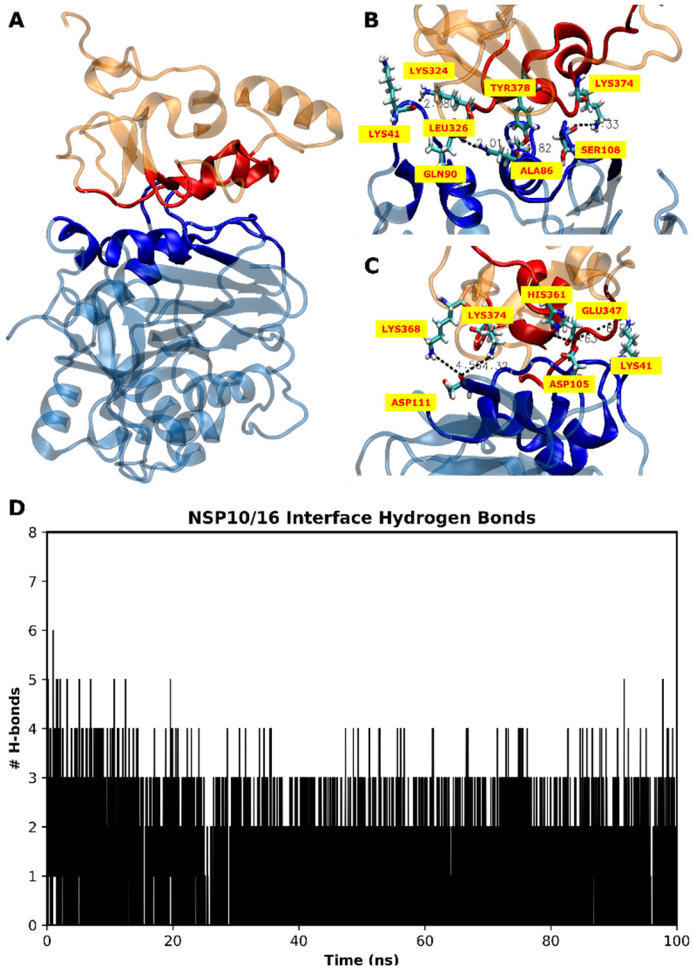

Figure S4. (A) 3D-representation of nsp10/16 dimer (PDB ID: 6W4H): nsp10 monomer (orange and its interface region in red, residues: 299 – 415) and nsp16 monomer (light blue and its interface region in dark blue, residues: 0 – 298) with an interface surface area of 19.5 nm^2; (B) H-bonds formed between the interface residues (> 25% occupancy are labelled); (C) Salt bridges formed between the interface residues (labelled) and (D) Total number of H-bonds formed between the interface residues during the MD simulation of nsp10/16 dimer. While there was a total of 6 unique H-bonds during the course of our MD, only an average of 3 were seen at a given time. This suggests the nsp10/16 interface is dynamic.

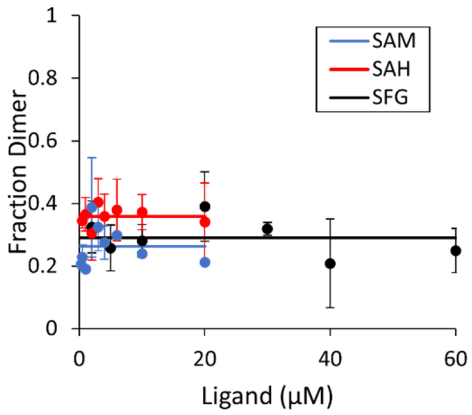

Figure S5. Fraction of protein dimer abundance over total protein abundance in MS spectra does not significantly change across the different ligand concentrations.

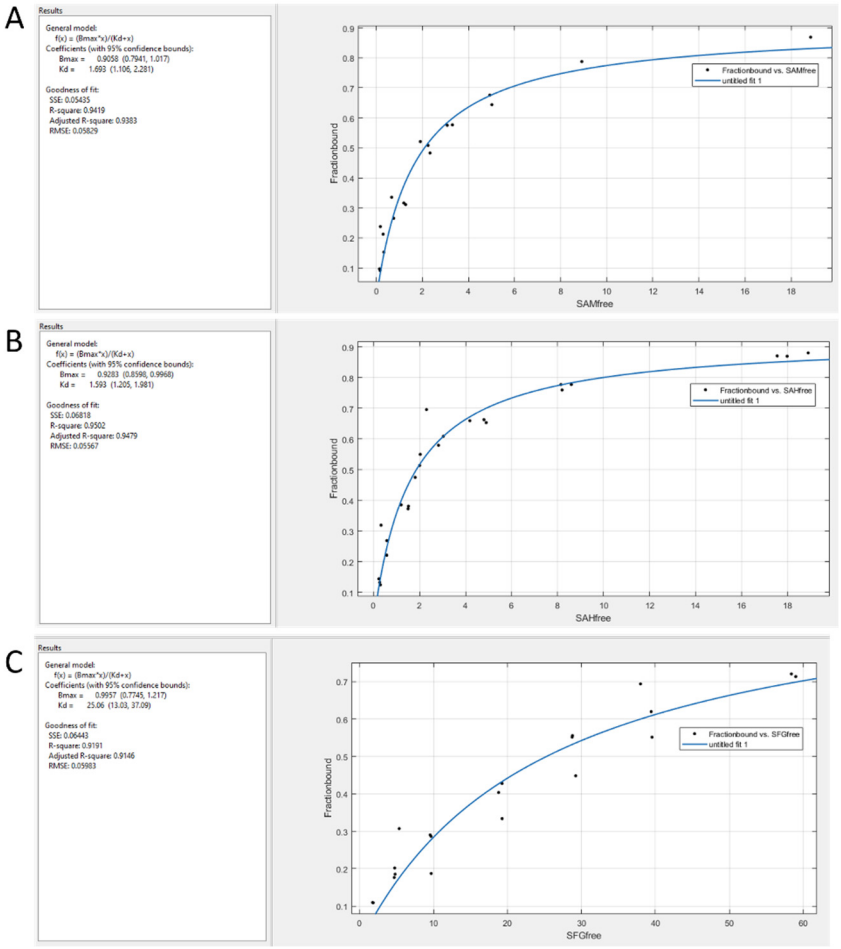

Figure S6. Curve fitting to calculate K_d of ligand binding using cftool in Matlab. The data were fit to the single-site binding model described in equation (2) based on the assumption that nsp10/16 dimer also displayed equal ionization efficiency at this total protein concentration and ligand binding did not significantly affect ionization efficiency over the ligand concentrations tested as shown in Figure S5. Curve fitting for titrations of (A) SAM, (B) SAH, and (C) SFG are depicted with calculated K_d values and 95 % confidence bounds of 1.7 µM (1.1, 2.3), 1.6 µM (1.2, 2.0), and 25 µM (13, 37), respectively. Individual calculated K_d values for each ligand titration data point show the binding affinity for 2 and 3 ligands bound (K_{d2} and K_{d3}) are at least an order of magnitude weaker than the calculated binding affinities for 1 ligand bound (K_{d1}), suggesting the additional ligand binding events are likely nonspecific in nature (see supplemental excel file uploaded with raw data). Since the goal of the work was to compare binding affinities between ligands, rather than obtain precise quantitative values, the apparent K_d values mentioned above are sufficient for comparison purposes.

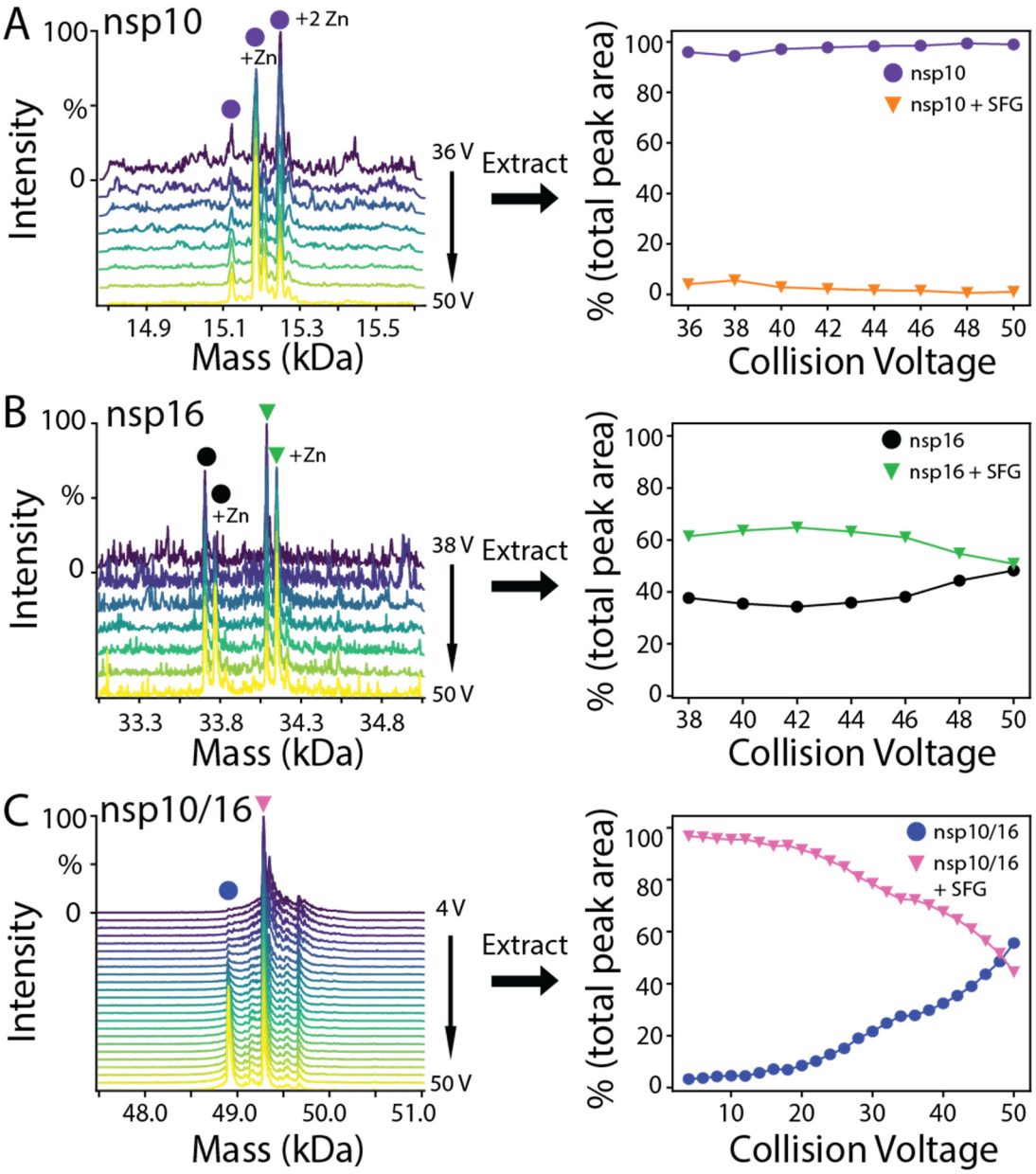

Figure S7. Collision induced dissociation of SFG from (A) dissociated nsp10 monomer, (B) dissociated nsp16 monomer, and (C) nsp10/16 heterodimer. Spectra were obtained in 2V CID increments from 4 – 50V, and then peak areas of the holo and apo peaks were extracted as a function of collision voltage. Insufficient S/N prevented accurate peak area calculations below 36V for nsp10, and below 38V for nsp16 (A and B). Upon dissociation from the SFG-bound nsp10/16 heterodimer, nsp10 monomer displayed no SFG binding (A). Additional peaks in the nsp10 spectra are due to bound Zn ions. Conversely, nsp16 monomer dissociated from the heterodimer with bound SFG, after which slight dissociation of SFG was observed as collision energy increased (B). As in the nsp10 spectra, additional peaks are the result of Zn binding. The nsp10/16 heterodimer lost SFG consistently as collision voltage was increased (C).

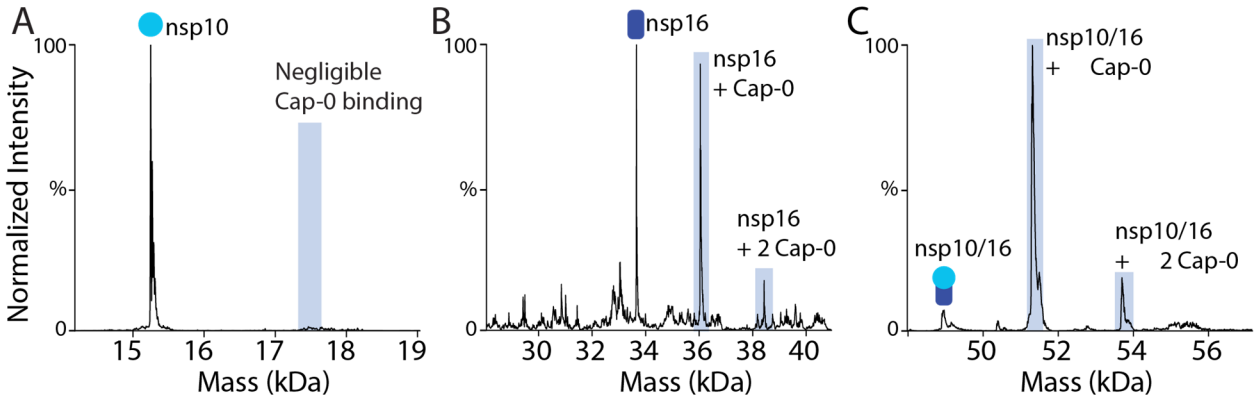

Figure S8. Cap-0 binding to (A) nsp10, (B) nsp16, and (C) nsp10/16. 2 µM cap-0 RNA (m^7GpppAUUAAA) was added to 5 µM protein. Nearly complete saturation (~96%) of the nsp10/16 heterodimer, ~47% binding to the nsp16 monomer, and negligible binding to nsp10 monomer was observed.

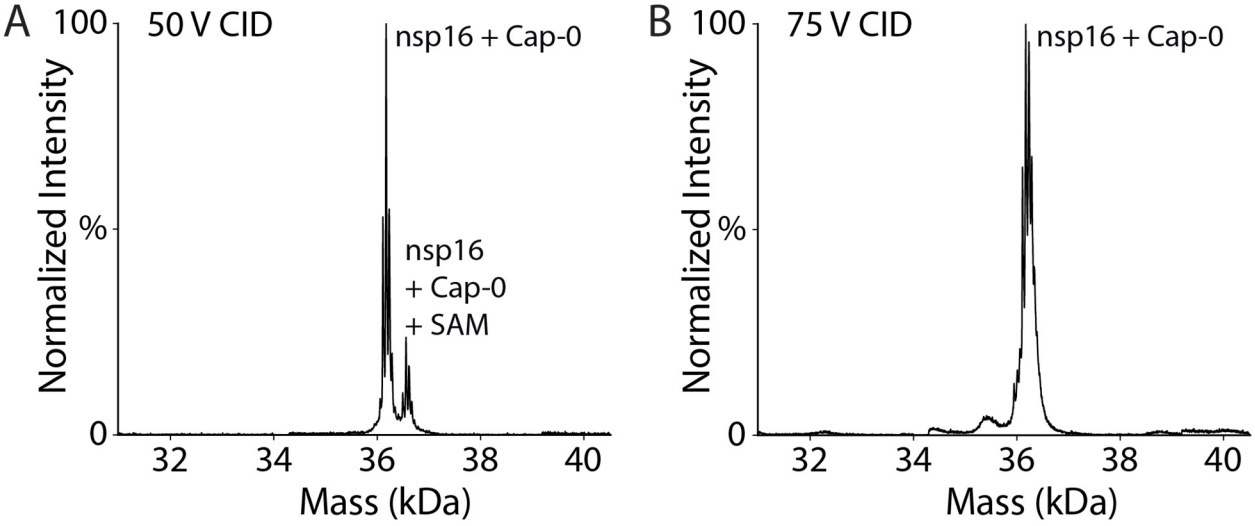

Figure S9. Deconvolved mass spectra showing the preservation of bound RNA for nsp16 released from SAM-bound dimer at 50V CID (A) and at 75V CID (B). Although SAM loss was significant, cap-0 RNA stable bound to the released nsp16.

(A) Cap-1: Cap-0 RNA with 4 µM SAM

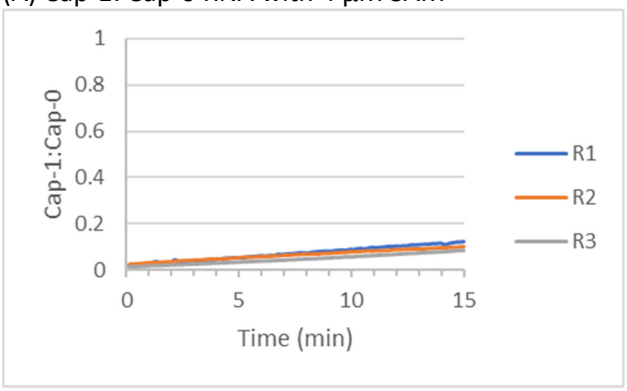

(D) SAH: SAM with 4 µM SAM

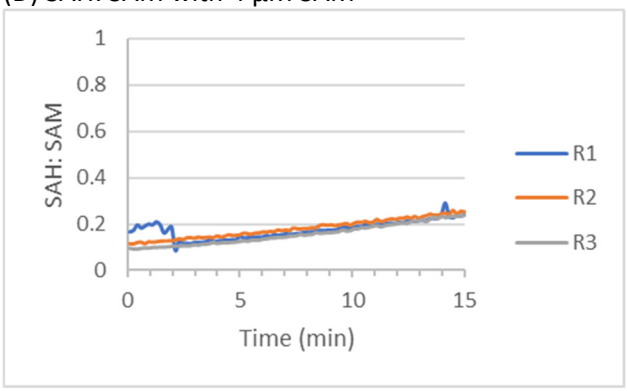

(B) Cap-1: Cap-0 RNA with 4 µM SAM + 100 µM Mn

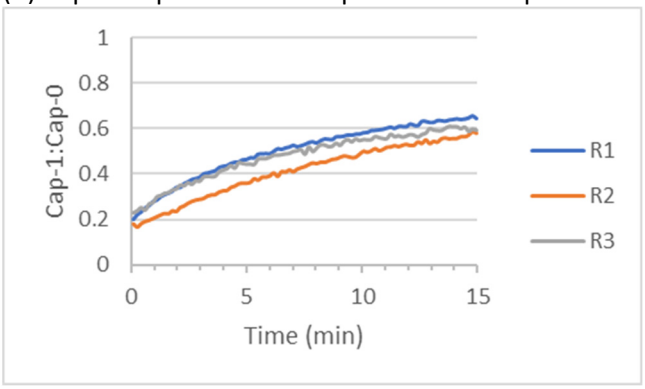

(E) SAH: SAM with 4 µM SAM + 100 µM Mn

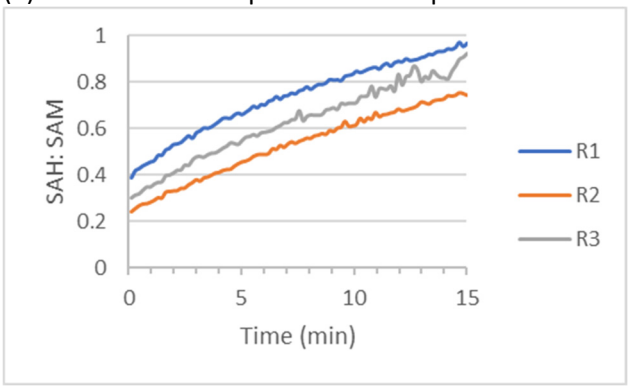

(C) Cap-1: Cap-0 RNA with 4 µM SAM + 100 µM Mn + 30 µM SFG

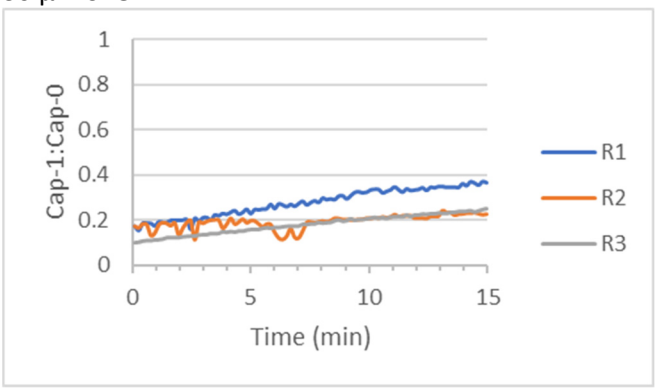

(F) SAH: SAM with 4 µM SAM + 100 µM Mn + 30 µM SFG

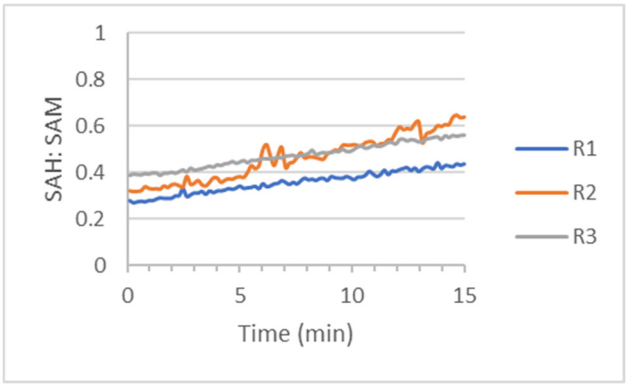

Figure S10. Monitoring increasing ratio of Cap-1: Cap-0 RNA when incubated with 0.25 mg/mL nsp10/16 enzyme plus (A) 4 µM SAM, (B) 4 µM SAM + 100 µM Mn, and (C) 4 µM SAM + 100 µM Mn + 30 µM SFG. The starting concentration of cap-0 RNA is 2 µM and the instrument conditions are the same as the data presented in the main text. The signal for the RNA peaks at *m/z* 1194 and 1201 were extracted using TWIMExtract (DOI: 10.1021/acs.analchem.7b00112) and plotted for 3 replicates in different colors. The methylation reaction proceeded the slowest in (A), and increased in presence of the known promoter Mn in (B). The expected inhibitory effect of SFG can be realized when comparing (B) and (C). The variation in the starting ratios was mostly due to varying sample mixing and loading time before the MS data acquisition. The reaction progress can also be seen by monitoring the ratio of the SAH: SAM peaks in the spectra at *m/z* 385 and 399 (D-F). Despite some signal variation, the plots demonstrate the potential of capturing the reaction kinetics in a quantitative manner in a single native MS experiment.